IEEE Access
Multidisciplinary ⋮ Rapid Review ⋮ Open Access Journal

Received August 31, 2020, accepted September 10, 2020, date of publication September 18, 2020, date of current version October 8, 2020.

Digital Object Identifier 10.1109/ACCESS.2020.3024733

Enhanced DVR Control System Based on the Harris Hawks Optimization Algorithm

ZEINAB ELKADY[1], NASER ABDEL-RAHIM[2], AHMED A. MANSOUR[1], AND FAHMY M. BENDARY[3]

[1]Electronics Research Institute, Cairo 11843, Egypt
[2]Future University, New Cairo 11835, Egypt
[3]Benha University, Banha 13518, Egypt

Corresponding author: Zeianb Elkady (zeinabelkady1985@gmail.com)

ABSTRACT The dynamic voltage restorer's (DVR) transient, steady-state, and dynamic responses are essential requirements for protecting sensitive loads against upstream voltage disturbances via the DVR's ride-through capabilities. DVRs also look after transient oscillation at the instant of entering, and /or exiting by the DVR. This paper presents an enhanced, optimized, and less complex DVR control system structure, which is capable of improving the transient, steady-state, and dynamic responses as well as eliminating inherent transient oscillations. The control system comprises a closed-loop feedback control signal and feedforward upstream disturbance detection signal. Incorporating the feedforward term helps, dramatically, in improving the system response and eliminating the transient oscillations in the load voltage. The error signals are adapted using a PI controller to make the load voltage faithfully track its predefined reference waveform. The controller is implemented in the dq synchronous rotating reference frame. The parameters of the PI controller are selected using modern population-based optimization called the Harris Hawks Optimization (HHO) technique. The results obtained using the HHO technique are compared with two other optimization algorithms, namely Particle Swarm Optimization (PSO) and Whale Optimization Algorithm (WOA). The results show that the HHO gives the best system response. The system is simulated using MATLAB/Simulink and the validation via Typhoon HIL402 real-time emulator. Both HIL402 validation and simulation results show that the proposed control scheme recovers normal operation against voltage disturbance within approximately 1.2 milliseconds without overshoot with steady-state error near zero and significantly dampens the inherent voltage oscillation that occurs at the instant of DVR entrance and/or exit.

INDEX TERMS Power quality, voltage source inverter, dynamic voltage restorer, voltage sag, voltage swell.

I. INTRODUCTION

Power quality (PQ) attracted much attention especially in industrial and commercial consumers due to the huge economic losses caused by poor PQ. With the expanding use of sensitive electronic equipment in the industrial, residential, and commercial sectors, voltage disturbances such as voltage sag (dip), voltage swell, flickers, interruptions, and voltage harmonics, have surfaced among the most significant PQ problems [1], [2]. According to some statistical studies, voltage sag has been identified as the most frequent and repeated voltage disturbance issue with a negative impact on production costs [3], [4]. Investigation of equipment sensitivity and malfunction occurring due to voltage dip has been reported in the literature [5]. Various examples of problems associated with different voltage sags have been discussed in [6], [7]. The causes of voltage sag/swell may be due to the starting of large motors or transformers energizing, switching operations, faults (short circuit), and sudden load changes [8]. Such causes are impossible to prevent but can be dealt with in a way to mitigate their negative impact on equipment.

Dynamic voltage restorer (DVR) is considered one of the most effective solutions for voltage sag and swell mitigation which is widely used in the industrial sector [7]. According to the IEEE 1346-1998 and IEEE 519-2014 standards [9], [10] a voltage sag/swell is defined as a decrease/increase in the RMS ac voltage (10–90% of the nominal voltage 110–190% of the nominal voltage), respectively, at the power frequency of

The associate editor coordinating the review of this manuscript and approving it for publication was Hao Luo.

duration from 10.0 milliseconds to 1.0 minute. From the definition, one of the most essential requirements in the voltage sag/swell compensation device is to detect and compensate the sag/swell within a time less than 10 milliseconds. Hence, the transient response and good overall performance of the DVR system are essential for providing good quality of the power system.

Several previous studies investigated the improvement of the DVR control system and the inherent problem of transient oscillation at the instant of DVR entrance and/or exit. Open-loop control was the most reported control strategy because of the fast voltage compensation requirement, but it was shown to have poor performance such as large steady-state error and long delay time in its response [11], [12]. Single-feedback closed-loop [13] and multi-feedback control loops [14] methods were applied to DVR in different studies aimed to improve the control system response. All of those studies succeeded in voltage compensation without indication of the transient response.

An integrated higher-order controller was implemented, based on ultra-capacitor (UCAP) DVR to improve the dynamic response of the DVR [15]. This technique was successful in voltage-sag compensation within 33 milliseconds. A proportional resonant controller for the current and voltage control loops was proposed to improve the transient response of the DVR in [16]. It has been reported that this proposed DVR control can compensate for the voltage sags within 20 milliseconds. In [17], a closed-loop state-variable control strategy in a multi-loop control structure was presented. The derivative of the output current was used to increase the dynamic response of the control system. That study compared the system behavior with open feed-forward and multi-loop structure counterparts and showed that the system achieved a better response in both transient and steady-state conditions. However, it required a current observer which complicated the control system. In [18], a repetitive control scheme for a series three-phase compensator was introduced. The controller response was delayed one PWM switching cycle. That response verified a very fast dynamic behavior, but the repetitive control scheme had an inherent drawback. Its performance could only be guaranteed when voltage disturbance followed certain repetitive scenarios.

This work proposes a less complicated system structure with reduced number of sensors while achieving enhanced dynamic, transient, and steady-state responses compared with other techniques in [15]–[18]. The proposed control incorporates one feedback control loop and one feedforward control loop. The feedforward control term determines the difference between the actual voltage at the point of common coupling (PCC) and its reference value. Incorporation of the feedforward term significantly improves the transient response of the DVR control system. Theeffectiveness of the feedforward term has been gradually introduced into the control loop to counteract overshoot at the instant of correction as well as undesirable oscillations in the system response. The feedback control loop compensates the difference between the actual load voltage and its reference waveform as well as the voltage drop caused by the DVR circuit itself.

Optimal tuning of the PI controllers' parameters has significantly enhanced the transient, dynamic, and steady-state response of the DVR. Three candidate optimization techniques, namely Harris Hawks Optimizer (HHO) [20], Particle Swarm Optimization (PSO) [19], and Whale Optimization Algorithm (WOA) [21], have been applied to the proposed controller in order to compare their performance. While the three techniques have yielded close results as far as steady-state performance is concerned, HHO, which has been selected for the proposed system, has offered superior performance in terms of transient response.

The system is simulated using MATLAB/Simulink and the simulation results show excellent response in transient, steady-state, and dynamic operation at different operating conditions. Verification of the proposed DVR control system is carried out using the Typhoon HIL 402 control centre in the virtual HIL SCADA system and via the hardware device in the laboratory.

The paper is organized as follows. The DVR power circuit, system modeling, and the control circuit structure are introduced in section 2. The PI controller tuning and performance index are illustrated in section 3. The problem formulation is presented in section 4. The simulation results and the system validation via typhoon HIL402 are introduced in section 5 and 6, respectively. Section 7 presents the conclusions of this paper.

II. SYSTEM DESCRIPTION

A. POWER CIRCUIT STRUCTURE

FIGURE 1. shows one of the most common configurations of the DVR power circuit [22]. The DVR is a series compensation device connected between the PCC and the sensitive load. The DVR power circuit consists of a controlled DC source, three-phase inverter, LC filter, and the injection transformer. In this study, the DVR is separately excited through a controlled DC link. The LC filter is an essential part to attenuate the high order harmonics caused by high-frequency pulse width modulation in the inverter. The injection transformer in the DVR systems guarantees galvanic isolation and filtration for the pulsating inverter output voltage. Careful design of the injection transformer is a very essential element in DVR as the transformer may reach saturation, overrating, and overheating issues [23].

In this study, it is assumed that the load is R-L with rated power 15.0 kVA at 0.95 lagging power factor and the DVR is designed to compensate the voltage dip/swell within $\pm$ 40% of the total kVA, i.e. the DVR is designed to compensate within $\pm$6.0 kVA. Considering that the primary side of the transformer is the inverter side, the transformer is a step-down transformer with turns' ratio 3:1 to decrease the current stress on the inverter switching devices. TABLE 1 illustrates the per phase system parameters.

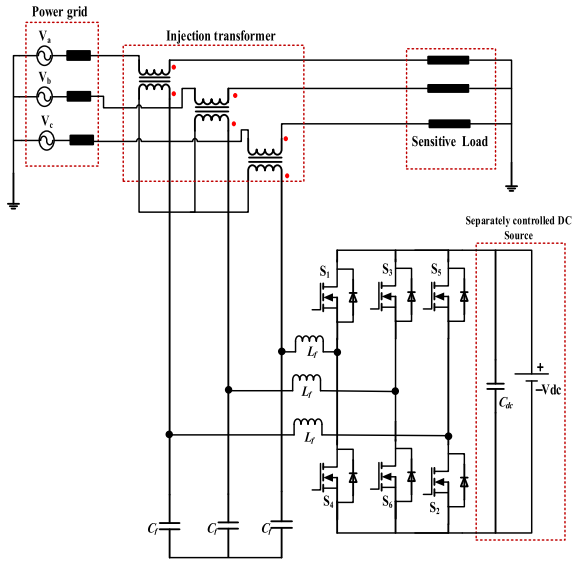

FIGURE 1. The power circuit of the system.

TABLE 1. System Parameters per Phase.

F_s (switching frequency	5.0 kHz
R (load)	10.0 Ω
L (load)	10.0 mH
Load power rating	4620.0 VA
Transformer rated power	6.0 kVA
Inverter rated power	2.5 kVA
L(filter)	2.0 mH
C (filter)	35 μF
Transformer turns ratio	3:1
$V_{primary}$ (inverter side)	350 V
$V_{secondary}$ (grid side)	117 V
V_{dc}	750.0 V
V_{PCC} (RMS phase value)	220.0 V

B. SYSTEM MODELING IN THE SYNCHRONOUS REFERENCE FRAME (SRF)

The equivalent circuit of the system model is shown in FIGURE 2. The DVR model is considered as an inverter with LCL filter as the inductance of the injection transformer is taken into consideration. Neglecting higher-order harmonics, the voltage source inverter (VSI) can be represented by an ideal AC ($V_{inv,a}$, $V_{inv,b}$, and $V_{inv,c}$) as depicted in FIGURE 2. Applying KVL yields

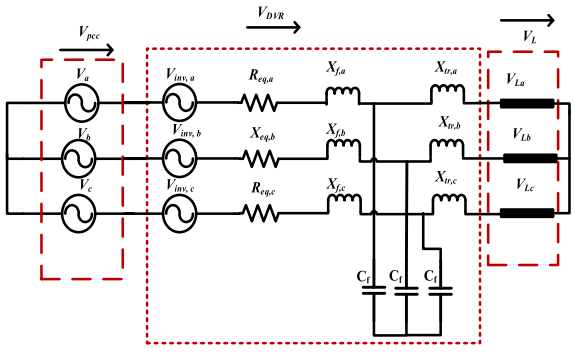

FIGURE 2. Simplified circuit model for the DVR.

$$\vec{V}_{L(a,\,b,\,c)} = \vec{V}_{PCC(a,\,b,\,c)} - \vec{V}_{DVR(a,\,b,\,c)} \quad (1)$$

$$\vec{V}_{DVR} = \vec{V}_{inv(a,\,b,\,c)} + \vec{I}_{a,b,c} \times Z_{eq} = \vec{V}_{PCC(a,b,c)} - \vec{V}_{L(a,b,c)} \quad (2)$$

where

- $\vec{V}_{PCC(a,\,b,\,c)}$ are the voltages of phase "a", "b", and "c" at the PCC, respectively,
- $\vec{I}_{a,b,c} \times Z_{eq}$ are the voltage drops over the DVR internal impedance (including the LC filter series inductance and the injection transformer impedance) for phases "a", "b", and "c", respectively,
- $\vec{V}_{inv(a,\,b,\,c)}$ are the controlled output voltage for phases "a", "b", and "c" of the VSI, respectively.

Equation (1) shows that the load voltage is dependent on the value of the voltage at the PCC (V_{pcc}) and the controlled DVR voltage (V_{DVR}). Equation (2) indicates that the compensation process should include compensation for the voltage drop over DVR internal impedance.

C. CONTROL SYSTEM STRUCTURE

1) BASIC CIRCUIT STRUCTURE

The main objectives of the DVR control system are as follows:

a) Detect the Grid angle (for grid synchronization),
b) Detect the load and/or grid voltages,
c) Calculate the reference voltage and the compensating voltage values,
d) Generate appropriate pulses for controlling VSI switching devices.

The voltage detection is carried out by measuring the instantaneous three-phase voltages $V_{a,b,c}$ at the PCC and at the load. Then, the three-phase voltages are transformed from the abc system to a two-phase stationary frame ($\alpha\beta$) system using Clark transformation as in (3). The transformation is based on the assumption that the α-axis is aligned with the phase "a"-axis and that the β-axis leads the α-axis with 90 degrees. The system voltages are then transformed from the stationary frame, $\alpha\beta$, to the rotating frame, dq, via Park transformation using (4) and as depicted in FIGURE 4. The grid angle (θ), used in (4), is obtained using the phase-locked loop, PLL, circuit shown in FIGURE 3.

FIGURE 3 illustrates the control structure of $\alpha\beta$-PLL stationary frame implemented on Matlab/Simulink platform. Notably, the $\alpha\beta$-PLL technique is widely used in three-phase grid-connected power converters because of its simple implementation and accurate estimation of the phase angle of the

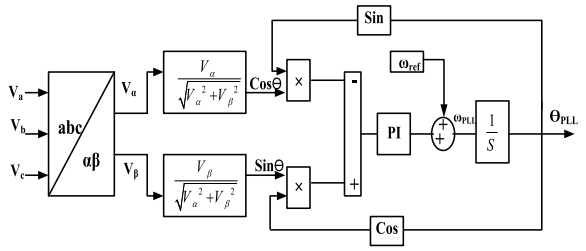

FIGURE 3. The control structure of $\alpha\beta$ PLL.

grid [24].

$$\begin{bmatrix} V_\alpha \\ V_\beta \\ V_o \end{bmatrix} = \frac{2}{3} \begin{pmatrix} 1 & -\frac{1}{2} & -\frac{1}{2} \\ 0 & \frac{\sqrt{3}}{2} & -\frac{\sqrt{3}}{2} \\ \frac{1}{\sqrt{2}} & \frac{1}{\sqrt{2}} & \frac{1}{\sqrt{2}} \end{pmatrix} \times \begin{bmatrix} V_a \\ V_b \\ V_c \end{bmatrix} \quad (3)$$

$$\begin{pmatrix} V_d \\ V_q \end{pmatrix} = \begin{pmatrix} \cos(\theta) & \sin(\theta) \\ -\sin(\theta) & \cos(\theta) \end{pmatrix} \times \begin{pmatrix} V_\alpha \\ V_\beta \end{pmatrix} \quad (4)$$

where

θ represents the transformation angle representing the vector position.

2) THE PROPOSED CONTROL ALGORITHM

Referring to (2), it can be seen that for good and fast dynamic responses, the voltage drop across the DVR, the voltage disturbance at the load side, as well as the disturbances in the voltage at PCC, are incorporated in the control loop. Referring to FIGURE 4, the principle of operation of the control system is as follows. The three-phase voltages $V_{a,b,c}$ at the PCC are transformed from the abc system to the $\alpha\beta$ system using Clark's transformation as in (3) and then to the dq system as in (4). The d-component of V_{PCC} ($V_{PCC,d}$, shown in FIGURE 4) is compared with its disturbance-free counterpart ($V^*_{pcc,d}$) to produce $e_{PCC,d}$. $e_{PCC,d}$ is passed through a rate limiter to regulate its influence on the control system response to eliminate load voltage overshoot. At the same time, the d-component of the load voltage ($V_{L,d}$) is compared with its reference value ($V^*_{L,d}$) to produce the error signal e_{vld}. e_{vld} is conditioned using the PI_1 controller to produce e_{cvld}. e_{cvld} is summed up with $e_{PCC,d}$ to produce e_{cd}. Meanwhile, the q-component of the load voltage ($V_{L,q}$) is compared with its reference value ($V^*_{L,q}$) to produce the error signal e_{vlq}. e_{vlq} is conditioned using the PI_2 controller to produce e_{cq}. Both e_{cd} and e_{cq} are transformed back to the $\alpha\beta$ system to produce V_α and V_β which are then employed to produce the proper space vector PWM signal. The PWM signal is used to control the switching devices of the voltage-source inverter (VSI). The output voltage of the VSI is stepped down using the series injection transformer to the power grid voltage level to produce the compensating voltage (V_{DVR}). V_{DVR} is summed up with V_{PCC} to produce the regulated load voltage.

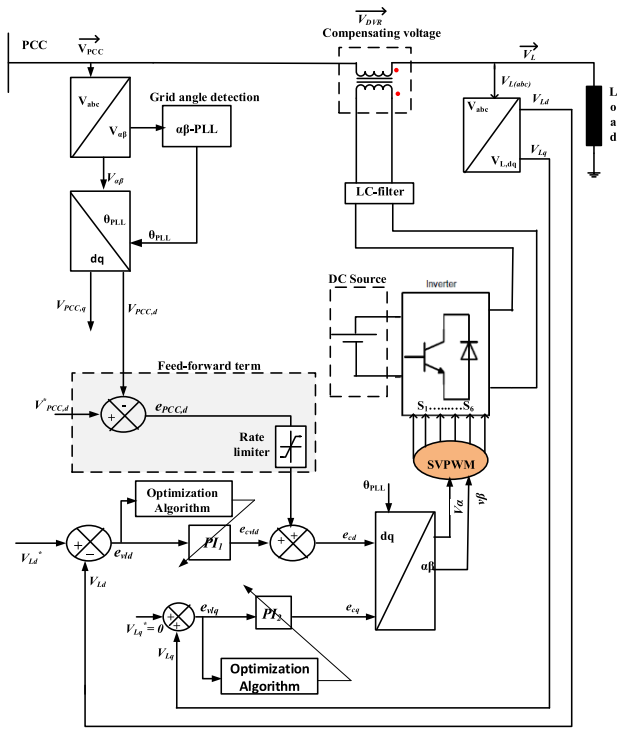

FIGURE 4. Structure of the DVR control scheme.

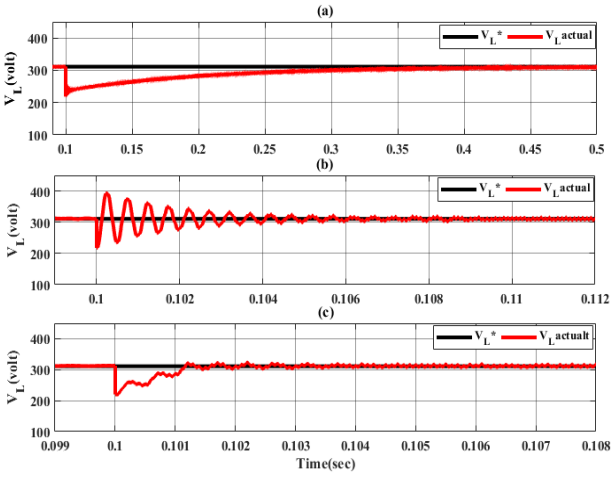

FIGURE 5. The control response (a) without feed-forward term, (b) with feedforward but without rate timer, and (c) the proposed control method.

FIGURE 5 shows the effect of incorporating the feedforward term (shown in FIGURE 4) within the control scheme. FIGURE 5.(a) shows that, without incorporating the feedforward term, the system takes about 450 milliseconds to reach a steady state. FIGURE 5.(b) shows that, when incorporating the feedforward term, the system reaches steady-state in approximately 6 milliseconds but with damped oscillations reaching as high as 25% of the steady-state voltage. FIGURE 5.(c) illustrates the effect of gradually introducing the feed-forward using the rate limiter. The controller

succeeds in reaching steady state within 1.2 milliseconds with almost no oscillations.

III. TUNING OF THE PI CONTROLLER PARAMETERS

The PI is a conventional controller that is commonly used in industrial applications because of its simple structure, low cost, and high stability margin. However, PI tuning is a difficult task, especially in the nonlinear dynamic systems. Recently, heuristic optimization techniques have been used for optimal tuning of PI controller gains [25], [26].

In the case of PI tuning via any optimization technique, some error criteria usually have to be minimized in order to reach optimal or near-optimal PI parameters. There are several performance criteria applied on different applications such as Integral Absolute Error (IAE), Integral of Square Error (ISE), Integral Time Absolute Error (ITAE), and Integral Time Square Error (ITSE) in response to a step function applied to the system input (setpoint) [27]. According to the nature of the application and the objective function, one of these criteria achieves the optimal solution [26]. The system is considered to be an optimal control system when the system parameters are adjusted in such a way that the indices reach, usually, a minimal value.

The ITAE criterion for the error signals (e_{vld} and v_{vlq}), is used as a performance index. This criterion helps to reach the optimal PIs controller parameters. Equations (5) and (6) represent the direct and quadrature error signals of the load voltage (see FIGURE 4).

$$e_{vld} = V^*_{Ld} - V_{Ld} \tag{5}$$

$$e_{vlq} = V^*_{Lq} - V_{Lq} \tag{6}$$

$$ITAE_d = \int_0^\infty t\,|e_{vld}|\,dt \tag{7}$$

$$ITAE_q = \int_0^\infty t\,\left|e_{vlq}\right|\,dt \tag{8}$$

where

V_{Ld}	is the actual d-component of the load voltage,
V_{Lq}	is the actual q-component of the load voltage,
V^*_{Ld}	is the reference of the d-component of the load voltage
V^*_{Lq}	is the reference of the q-component of the load voltage

The selection of the PI parameters is carried out using the HHO algorithm which was found to offer the most optimum parameters when compared to other optimization techniques, namely PSO and WOA. The following three sections present the application of the three optimization techniques for selecting the parameters of the PI controllers.

A. THE PARTICLE SWARM OPTIMIZATION (PSO)

The idea of the PSO was inspired by the behavior of animals such as fish schooling and birds flocking [28]. Each animal position (particle position) and velocity is updated to the best position and guided toward the best position in the search space. The PSO mathematical equations can be represented by (9)-(11).

$$Vi(k+1) = \beta\, Vi(k) + d_1 r_1\,(pi, best(k) - xi(k)) + d_2 r_2\,(G_{best}(k) - xi(k)) \tag{9}$$

$$xi(k+1) = xi(k) + vi(k+1) \tag{10}$$

$$\beta\,(t) = \beta_{max} - \left(\frac{(\beta_{max} - \beta_{min})}{\max\_iter}\right) \tag{11}$$

where

$V_i(k)$	is the velocity of particle,
$X_i(k)$	is the position of particle i,
$P_{i,best}$	is the best position of until iteration k,
I	is the number of particles,
K	number of iterations,
β	particle inertia;
d_1	social attraction;
d_2	cognitive attraction;
r_1, r_2	uniform random numbers.

1) THE WHALE OPTIMIZATION ALGORITHM (WOA)

WAO is a nature-inspired meta-heuristic algorithm presented in [21]. The method of searching consists of two stages, exploration and exploitation. In the former stage, the algorithm explores the global search space. The latter stage follows the exploration and investigates in detail the optimal values of PI controllers K_{p1}, K_{i1}, K_{p2}, and K_{i2}.

$$\overrightarrow{D} = \left|\overrightarrow{C} \times \overrightarrow{X^*}(t) - \overrightarrow{X}(t)\right| \tag{12}$$

$$\overrightarrow{X}(t+1) = \overrightarrow{X}^*(t) - \overrightarrow{A} \times \overrightarrow{D} \tag{13}$$

where

t	indicates the current iteration,
$\overrightarrow{A}$ and $\overrightarrow{C}$	are coefficient vectors,
$\overrightarrow{X^*}$	is the position vector

B. THE HARRIS HAWKS OPTIMIZATION (HHO)

The HHO is a metaheuristic optimization technique that mimics the cooperative activity of an effective chasing style of Harris Hawks called "surprise pounce" [29], [20]. Like other metaheuristic algorithms, the HHO algorithm also contains the phases of exploration and exploitation. HHO is a population-based, gradient-free optimization technique. Therefore, it can be used with proper formulation for any optimization problem. The HHO algorithm includes two exploration phases and four exploitative steps. Moreover, the mathematical representation of this cooperative activity suggests a new stochastic approach to deal with several optimization problems [30]. The next section illustrates how the HHO technique is applied to the proposed DVR control system.

1) EXPLORATION PHASE

In this stage, HHO remains in certain areas randomly hoping to find the prey based on two tactics. The position of each hawk is adjusted by an equation, (14). In our situation, the "preys" are the PI controller parameters K_{p1}, K_{i1}, K_{p2}, and K_{i2} and the "hawks" are the number of search agents that have been proposed.

$$Y(t+1) = \begin{cases} (Y_{prey}(t) - Y_m(t)) - c_3(LB + c_4(UB - LB)), & K < 0.5 \\ Y_{rand}(t) - c_1 \left| Y_{rand}(t) - 2c_2 Y(t) \right|, & K \geq 0.5 \end{cases} \quad (14)$$

where:

$Y(t+1)$	is the position vector of hawks in the next iteration,
$Y_{prey}(t)$	is the position of prey (K_{p1}, K_{i1}, K_{p2}, and K_{i2}),
K, c_1, c_2, c_3, c_4	are random numbers inside (0,1) updated in each iteration,
$Y(t)$	is the current position vector of hawks, c_1, c_2, c_3, c_4,
$Y_{rand}(t)$	is a randomly selected hawk from the current population,
LB & UB	are the lower and upper bounds of variables, representing the expected minimum and maximum values K_{p1}, K_{i1}, K_{p2}, and K_{i2}.

The hawks reach an average position via equation (15),

$$Ym(t) = \frac{1}{N} \sum_{i=1}^{N} Yi(t) \quad (15)$$

where:

$Y_m(t)$	is the average position of the hawks,
$Y_i(t)$	is the location of each hawk in iteration t,
N	is the total number of hawks (no of search engines here, $N = 10$).

2) TRANSITION FROM EXPLORATION TO EXPLOITATION

Since the prey tries to escape, there is a process between exploitation and discovery called the transition from exploration to exploitation. The prey loses a lot of energy during its attempt to escape. The prey's energy equation is modeled in equation (16):

$$E = 2E_o(1 - \frac{t}{T}) \quad (16)$$

where,

E	indicates the escaping energy of the prey,
T	is the maximum number of iterations, and
E_0	is the initial state of its energy.

3) EXPLOITATION PHASE

a: SOFT BESIEGE ($R \geq 0.5$ AND $|E| \geq 0.5$)

The Harris's hawks encircle the prey quietly to exhaust it before the hawks swoop on it. This action is described by equations (17) and (18)

$$Y(t+1) = \Delta Y(t) - E \left| KY_{prey}(t) - Y(t) \right| \quad (17)$$

$$\Delta Y(t) = Y_{prey}(t) - Y(t). \quad (18)$$

where

$\Delta Y(t)$	is the difference between the position of the prey and the current location of the hawk in iteration t.
K	refers to the strength of the prey randomly jumping during the escape $k = 2(1\text{-}c_5)$. In each iteration, this value changes randomly to simulate the nature of prey movements.
r	is the prey's chance of successfully escaping.

b: HARD BESIEGE ($R \geq 0.5$ AND $|E| < 0.5$)

In this case, the prey becomes too exhausted to escape. As a result, the hawks effortlessly catch the prey, and then pounce on it. Using (19), each hawk upgrades its current location.

$$Y(t+1) = Y_{prey}(t) - E \left| \Delta Y(t) \right| \quad (19)$$

c: SOFT BESIEGE WITH PROGRESSIVE RAPID DIVES

In this approach, assume that the hawks could evaluate (decide) their next move based on the following rule

$$H = Y_{prey}(t) - E \left| k\, Y_{prey}(t) - Y(t) \right| \quad (20)$$

In the HHO algorithm, the concept of Lévy Flight (LF) is used to design a mathematical model that illustrates the zigzag movement of the prey during its attempt to escape. The hawks are supposed to dive towards the prey based on the *LF* rule in (21). Equations (22) and (23) are used to calculate the *LF* function.

$$G = H + S \times LF(D) \quad (21)$$

$$LF(x) = 0.01 \times \frac{u \times \sigma}{|v|^{\frac{1}{\beta}}} \quad (22)$$

$$\sigma = \left(\frac{\Gamma(1+\beta) \times \sin\left(\frac{\pi\beta}{2}\right)}{\Gamma\left(\frac{1+\beta}{2}\right) \times \beta \times 2^{\left(\frac{\beta-1}{2}\right)}} \right)^{\frac{1}{\beta}} \quad (23)$$

where,

D	is the dimension of the problem,
S	is a random vector by size $1 \times D$,
LF	is the Lévy flight function.

d: HARD BESIEGE WITH PROGRESSIVE RAPID DIVES

The position of team members is updated by reducing the distance between their average position and the prey position. This motion is illustrated by (24)

$$Y(t+1) = \begin{cases} H \text{ if } F(H) < F(Y(t)) \\ G \text{ if } F(G) < F(Y(t)), \end{cases} \quad (24)$$

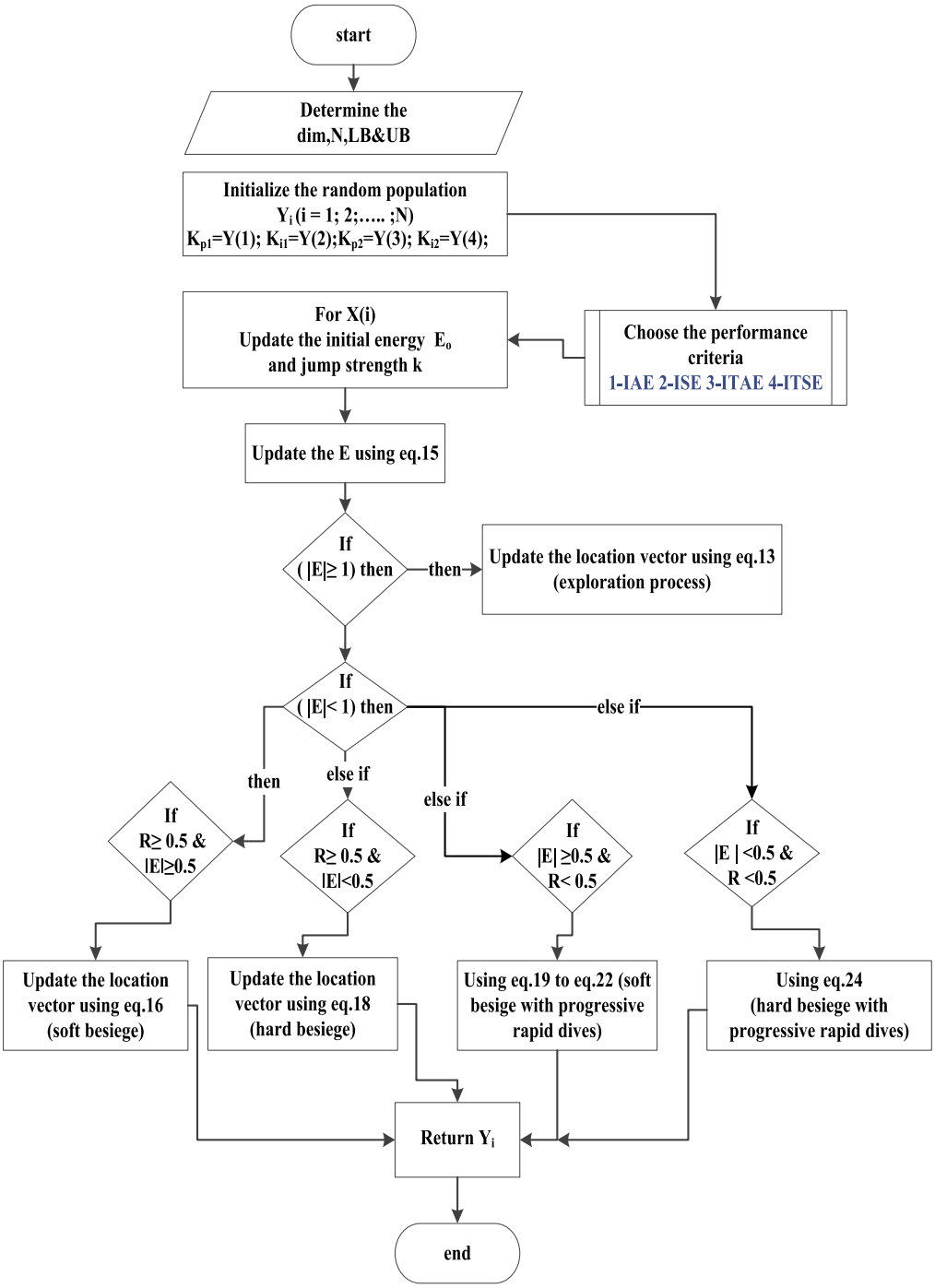

FIGURE 6. The flow chart of the HHO algorithm applied to the proposed DVR control system.

where H and G are obtained by applying new rules represented by (25) and (26):

$$H = Y_{\text{prey}}(t) - E\left|kY_{\text{prey}}(t) - Y_m(t)\right| \quad (25)$$

$$G = H + S \times LF(D). \quad (26)$$

where, Y_{m}(t) is obtained from equation (15)

FIGURE 6 demonstrates a flow chart for the application of the HHO algorithm on the proposed DVR control system.

IV. PROBLEM FORMULATION

In this work, HHO is compared against two evolutionary algorithms, WOA and PSO, to select optimal parameters for the PI controllers. The problem formulation for the proposed DVR control system is based on the objective function given by (7) and (8) to minimize the time-absolute-integral of error.

The HHO delivers the best performance as far as transient response is concerned. TABLE 2 provides selected results

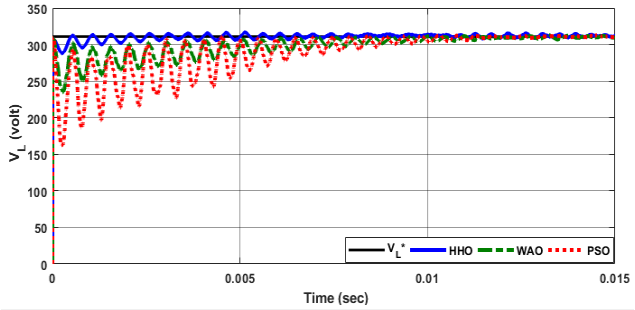

FIGURE 7. Transient response of three optimization techniques, PSO, WAO, and HHO.

TABLE 2. Selected Results of the Applied Technique.

	PSO	WAO	HHO
K_{p1}	0.924968	0.789503	0.944475
K_{i1}	26.6356	33.2409	47.9099
K_{p2}	0.757342	0.298891	0.0269796
K_{i2}	4.41094	13.0096	6.95262
The objective function	4551.66	4521.19	4501.48

of the optimal solutions for three optimization methods. FIGURE 7 depicts the transient response for the DVR using the controller parameters based on the optimal solutions from the three methods. The HHO provides the best result without over-shooting, the lowest settling time ≈ 1 milliseconds, and minimal steady-state error. By contrast, PSO and WAO give settling times ≈10 milliseconds and ≈ 5 milliseconds, respectively.

V. SIMULATION RESULTS

The three-phase DVR closed-loop control scheme depicted in FIGURE 4 is simulated using Matlab/Simulink. The system parameters are given in TABLE 1. FIGURE 8 shows the system performance when tested against ±30% disturbance of the nominal voltage at the PCC. FIGURE 8.(a) shows the voltage at PCC at nominal operation from t = 0 to 0.1 seconds (peak value of $V_{PPC} = V_L = 311$Volts). At t=0.1 sec. to t=0.2 sec., V_{PCC} undergoes a voltage sag of ≅-30% of its nominal voltage to reach a peak value of 217.7 Volts. For the same time interval, the DVR produces an aiding voltage that counteracts this voltage sag (FIGURE 8.(b)) to result in a load voltage that is almost free of disturbances (FIGURE 8.(c)). From t=0.2 to t=0.3, the system regains its nominal operating conditions. At t=0.3 seconds to t=0.4 seconds, the voltage at the PCC undergoes a voltage swell of ≅ +30% of its nominal voltage to reach as high as 404.5 Volts. For the same time interval, the DVR produces an opposing voltage that counteracts this voltage swell and results in a load voltage that is almost disturbance-free. FIGURE 9 shows a zoomed-in view for FIGURE 8 during the sag interval and at

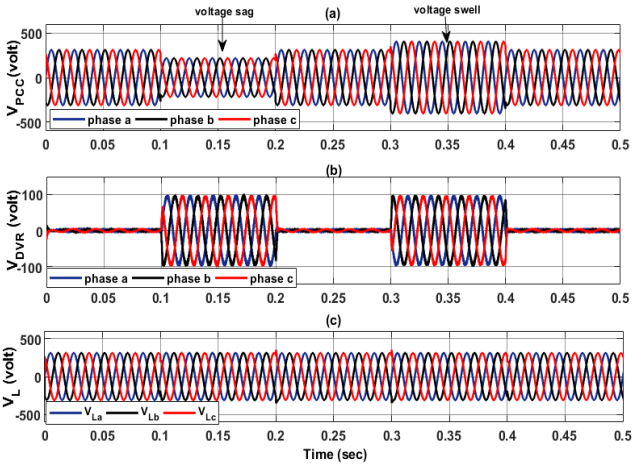

FIGURE 8. Three-phase sinusoidal voltages during balanced sag and swellat the PCC.

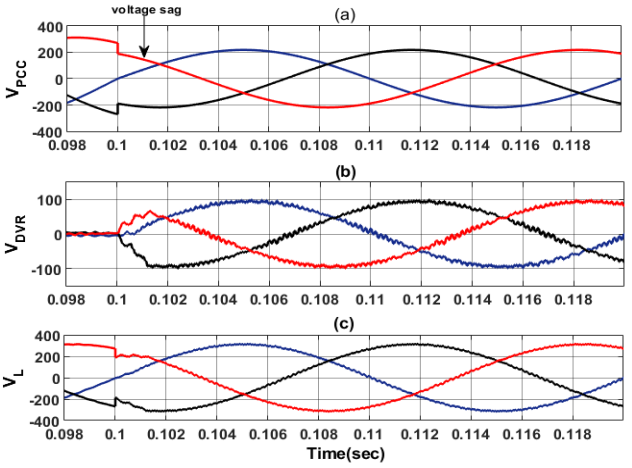

FIGURE 9. Zoomed-in view indicating the damping oscillation at the instant of DVR entrance.

the commencement of the DVR corrective action (the start of the compensation process) which usually results in damped oscillation at the load [17]. FIGURE 9 (c) indicates that the load voltage was compensated with almost no oscillations. This indicates that the proposed control system succeeds in mitigating the oscillation caused at the instant of DVR entrance and /or exit.

FIGURE 10 depicts the dynamic response of the load voltage during voltage sag. The inner window provides a zoomed-in view of the disturbance interval. It is shown that the proposed system takes about 1.2 milliseconds to reach steady-state and counteract the disturbance. The inner window in FIGURE 11 shows a zoomed view of the dynamic response at the start of swell disturbance. The figure shows that the system takes approximately 1.1 milliseconds to recover from the swell disturbance with near zero steady-state error. These results indicate that the controller is capable of coping with system disturbances which may occur at

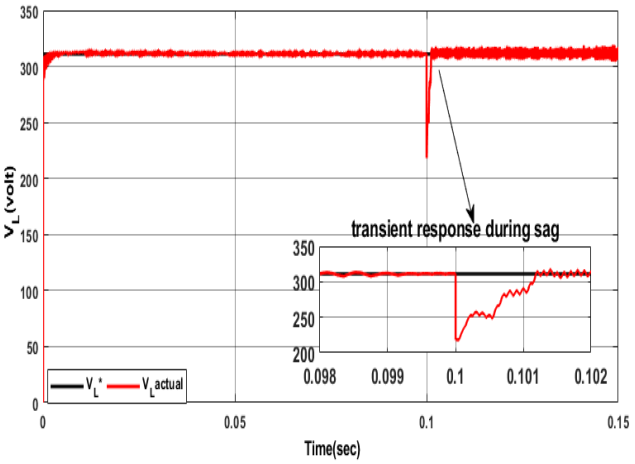

FIGURE 10. Zoom view indicates the dynamic response of the control system during voltage sag.

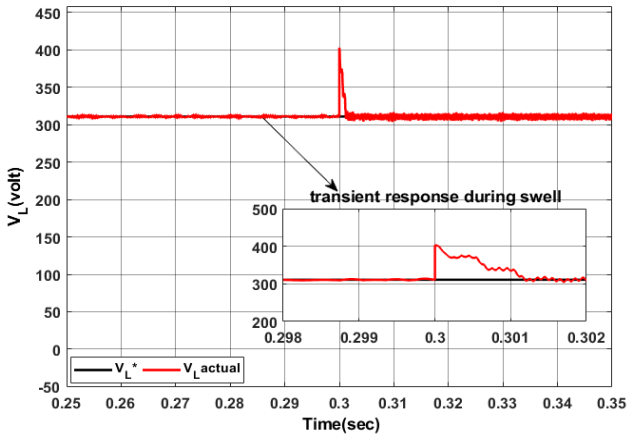

FIGURE 11. Zoomed-in view indicating the dynamic response of the proposed controller during voltage swell.

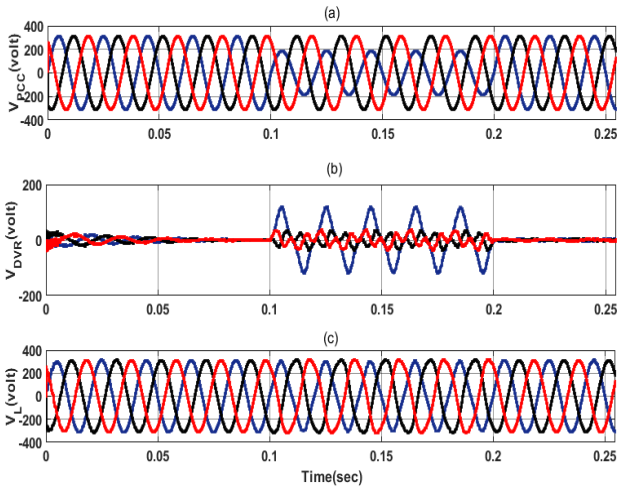

FIGURE 12. Unbalanced voltage sag compensation for only one phase.

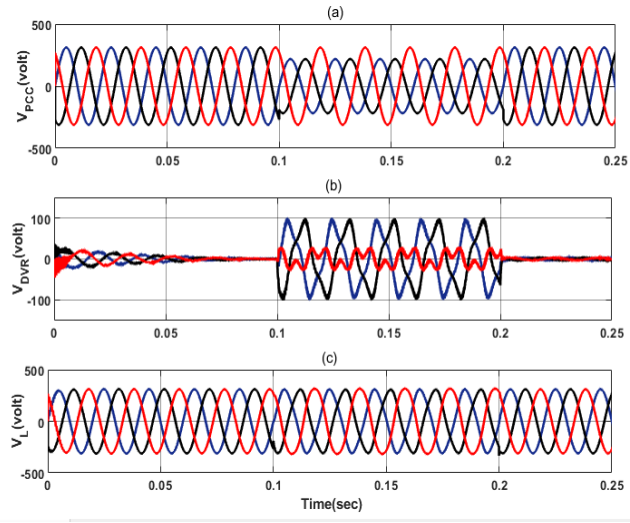

FIGURE 13. Unbalanced voltage sag for two phases.

the source side with excellent dynamic and steady-state responses.

FIGURE 12 and FIGURE 13 show the DVR's behavior for unbalanced voltage sags. In FIGURE 12, only phase "a" voltage undergoes a sag of −30% from its nominal value.

In FIGURE 13, the voltage sag affected the two phases equally by -30 % from their nominal value. The figure indicates that the system is capable of effectively dealing with unbalanced sags.

FIGURE 14 presents the active and reactive power before, during, and after sag and swell at the PCC. The figure shows that there is a reduction in active and reactive power delivered by the PCC during the sag and increase in the active and reactive power during the swell. FIGURE 15 indicates the DVR active and reactive power compensation during sag and swell. The figure shows that DVR injects and absorbs power during voltage sag and voltage swell, respectively.

FIGURE 16 shows that the load almost suffers no voltage disturbances in the power delivered to it throughout all upstream abnormalities. This indicates that DVR effectively mitigates sag and swell occurrences as shown in TABLE 3.

FIGURE 17 and FIGURE 18 depict the RMS and the three-phase sinusoidal currents at various points in the system. FIGURE 19 shows the system behavior at other ratios of voltage sag and the corresponding compensation. As depicted, the DVR can isolate the load from any disturbance (swell/sag) that might occur at the PCC by providing the proper voltage compensation.

VI. EXPERIMENTAL VALIDATION BASED ON TYPHOON HIL402

Hardware-in-the-Loop (HIL) real-time emulators are extensively used for power electronics control system design, testing, and test automation. A real-time emulator for the

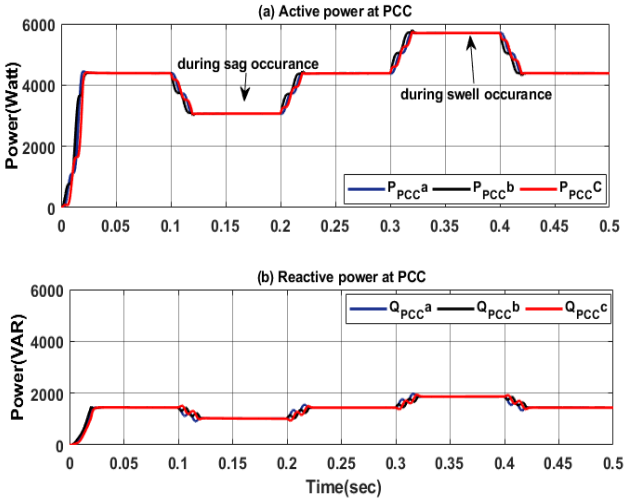

FIGURE 14. Active and reactive power at the grid side.

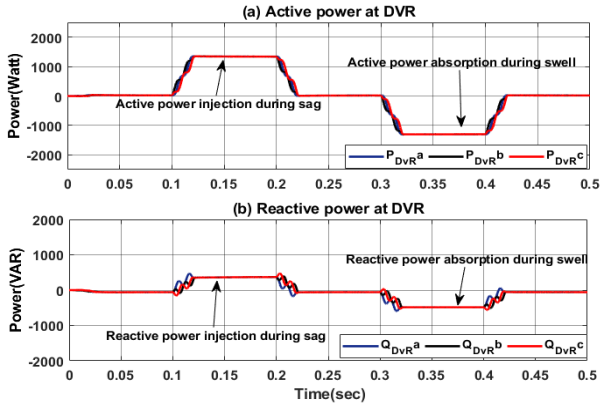

FIGURE 15. Active and reactive power injected by the DVR.

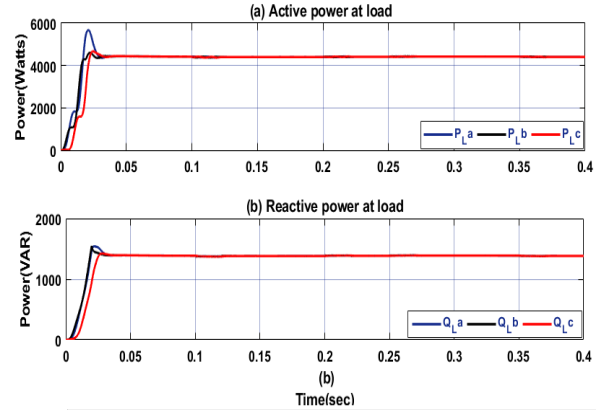

FIGURE 16. Active and reactive power at the load side.

proposed DVR control structure is performed via the Typhoon HIL402 kit through a breakout board [31], [32]. FIGURE 20 presents a photo of the setup system using the HIL402 kit and

TABLE 3. Power flow in the proposed system.

Power Status	Power at the grid side	Power injected by DVR	Load power
Without sag/swell	P≈3900 watt Q≈2500 var	P≈500 watt Q≈-1100 var	P≈4400 watt Q≈1390 var
During sag	P≈2660 watt Q≈1800var	P≈1740 watt Q≈-420var	P≈4400 watt Q≈1380 var
During swell	P≈5000 watt Q≈3200 var	P≈-600 watt Q≈-1800 var	P≈4400 watt Q≈1400 var

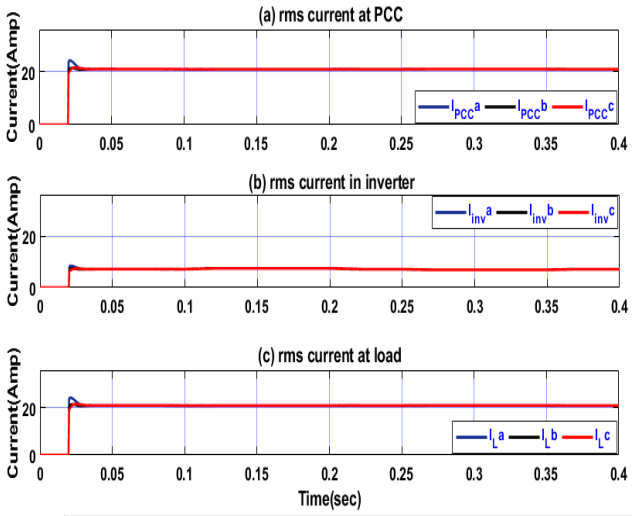

FIGURE 17. RMS currents in the proposed system.

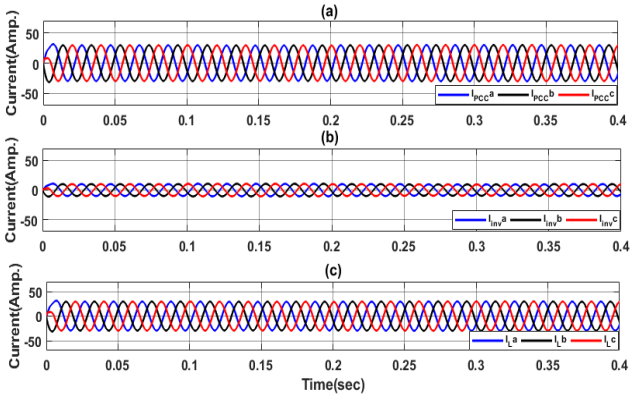

FIGURE 18. Three-phase sinusoidal currents in the proposed system: (a) at the PCC, (b) at the DVR, (c) at the load.

a breakout board to test the proposed system. The DVR power and control circuits are modeled on the Typhoon HIL control center schematic editor.

FIGURE 21 and FIGURE 22 show the system behavior during sag and swell. Channels A and B display a single-phase grid voltage and load voltage, respectively. Channels C and D display the reference load voltage and the actual load voltage, respectively. FIGURE 23 represents a zoomed-in view for the control response which is in very close agreement

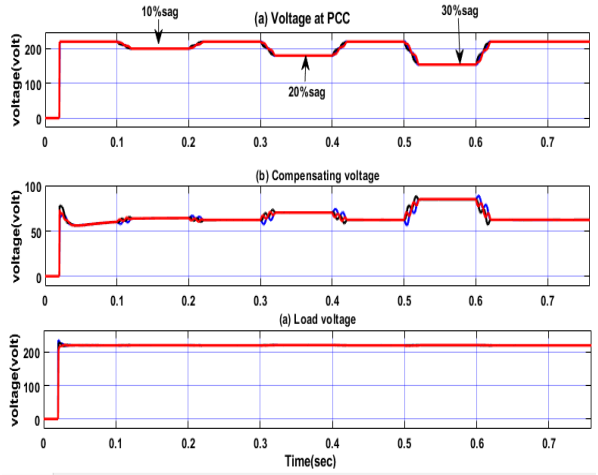

FIGURE 19. Different ratios of sag values and corresponding compensation.

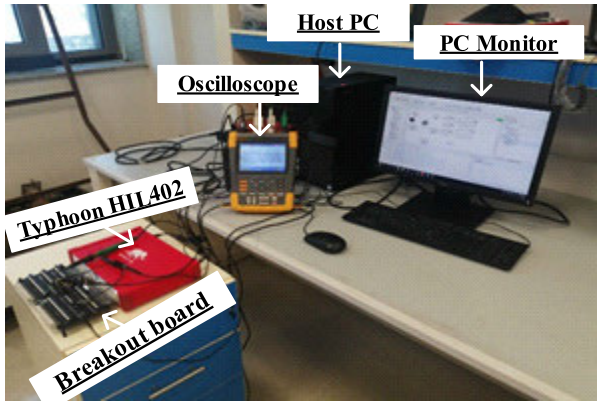

FIGURE 20. Photo of the setup of the system implementation based on Typhoon HIL 402.

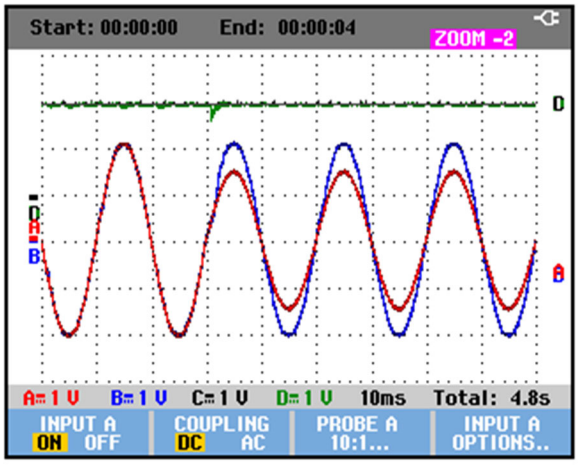

FIGURE 21. Four-channel scope view displays the instant of sag occurrence.

with the simulation results. The figure also indicates that the proposed control structure compensates for the voltage disturbance within $\approx$ 1.2 milliseconds.

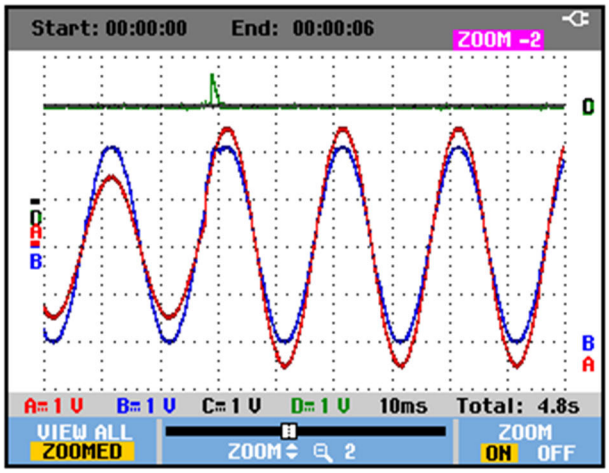

FIGURE 22. Four-channel scope view displays the instant of swell occurrence.

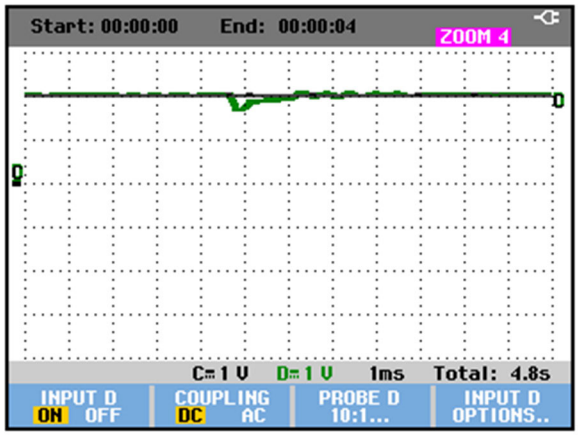

FIGURE 23. Scope zoom view represent the actual and reference load voltage.

VII. CONCLUSIONS

This paper proposed an enhanced, optimized, and less complex control structure for the Dynamic Voltage Restorer (DVR) that achieved excellent protection against load voltage sag and/or swell. Combining the feedforward upstream disturbance detection term and the closed-loop feedback control signal helped in improving the transient response and eliminating undesirable transient oscillation at the instant of DVR compensation. Tuning the PI controller parameters was based on the Harris Hawks Optimization (HHO), which was found to offer the most optimal PI parameters for the proposed controller when compared against two other optimization algorithms, namely PSO and WAO. Simulation results using MATLAB/Simulink indicated that the proposed control scheme recovered normal operation against voltage disturbance within approximately 1.2 milliseconds without overshoot and with steady-state error near zero and significantly dampened the inherent voltage oscillation at the instant of DVR entrance or exit. Validation of the proposed

DVR control structure was performed via Typhoon HIL402. The validation results were in good agreement with those of MATLAB simulation.

REFERENCES

[1] M. H. J. Bollen, *Understating Power Quality Problems: Voltage Sags and Interruptions*. New York, NY, USA: Wiley, 1999.
[2] A. B. Mohammed, M. Aifaa, and M. Ariff, "The enhancement of power quality for the distribution system via dynamic voltage restorer," *Int. J. Power Electron. Drive Syst.*, vol. 11, no. 3, pp. 1588–1595, 2020.
[3] S. A. Rahman and E. Dagnew, "Voltage sag compensation using direct converter based DVR by modulating the error signal," *Indonesian J. Electr. Eng. Comput. Sci.*, vol. 19, no. 2, pp. 608–616, 2020.
[4] *IEEE Recommended the Practice for Evaluating Electric Power System Compatibility With Electronic Process Equipment*, IEEE Standard 1346, 1998.
[5] J. Prousalidis, E. Styvaktakis, E. Sofras, I. K. Hatzilau, and D. Muthumuni, "Voltage dips in ship systems," in *Proc. IEEE Electr. Ship Technol. Symp.*, May 2007, pp. 309–314.
[6] A. Iagar, G. N. Popa, and C. M. Dinis, "Investigation of power quality problems at a wood-based panels plant," in *Proc. 10th Int. Symp. Adv. Topics Electr. Eng. (ATEE)*, 2017, pp. 579–584.
[7] M. H. J. Bollen, "Voltage sags: Effects, mitigation, and prediction," *Power Eng. J.*, vol. 10, no. 3, pp. 129–135, Jun. 1996.
[8] C. Tu, Q. Guo, F. Jiang, H. Wang, and Z. Shuai, "A comprehensive study to mitigate voltage sags and phase jumps using a dynamic voltage restorer," *IEEE J. Emerg. Sel. Topics Power Electron.*, vol. 8, no. 2, pp. 1490–1502, Jun. 2020.
[9] *IEEE Recommended Practice for Evaluating Electric Power System Compatibility With Electronic Process Equipment*, IEEE Standard 1346, 1998.
[10] *IEEE Recommended Practice and Requirements for Harmonic Control in Electric Power Systems*, IEEE Standard 519-2014, Jun. 11, 2014, pp. 1–29.
[11] T. A. J. Kara, M. Rahmani, and D. Westermann, "Power quality ensured by dynamic voltage correction," *ABB Rev.*, vol. 4, pp. 25–36, Apr. 1998.
[12] J. G. Nielsen, F. Blaabjerg, and N. Mohan, "Control strategies for dynamic voltage restorer compensating voltage sags with phase jump," in *Proc. 16th Annu. IEEE Appl. Power Electron. Conf. Expo. (APEC)*, vol. 2, Mar. 2001, pp. 1267–1273.
[13] M. Vilathgamuwa, A. A. D. R. Perera, S. S. Choi, and K. J. Tseng, "Control of energy optimized dynamic voltage restorer," in *Proc. 25th Annu. Conf. IEEE Ind. Electron. Soc. (IECON)*, vol. 2, Nov. 1999, pp. 873–878.
[14] M. Vilathgamuwa, A. A. D. Ranjith Perera, and S. S. Choi, "Performance improvement of the dynamic voltage restorer with closed-loop load voltage and current-mode control," *IEEE Trans. Power Electron.*, vol. 17, no. 5, pp. 824–834, Sep. 2002.
[15] D. Somayajula and M. L. Crow, "An integrated dynamic voltage restorer-ultracapacitor design for improving power quality of the distribution grid," *IEEE Trans. Sustain. Energy*, vol. 6, no. 2, pp. 616–624, Apr. 2015.
[16] P. Vu, N. Dinh, N. Hoang, Q. Nguyen, D. Nguyen, and M. Tran, "A generalized parameter tuning method of proportional- resonant controllers for dynamic voltage restorers," *Int. J. Power Electron. Drive Syst.*, vol. 9, no. 4, pp. 1709–1717, 2018.
[17] G. Joos, S. Chen, and L. Lopes, "Closed-loop state variable control of dynamic voltage restorers with fast compensation characteristics," in *Proc. Rec. IEEE Ind. Appl. Conf., 39th IAS Annu. Meeting.*, vol. 4, Oct. 2004, pp. 2252–2258.
[18] D. A. Fernandes, F. F. Costa, J. R. S. Martins, A. S. Lock, E. R. C. da Silva, and M. A. Vitorino, "Sensitive load voltage compensation performed by a suitable control method," *IEEE Trans. Ind. Appl.*, vol. 53, no. 5, pp. 4877–4885, Sep. 2017.
[19] R. Eberhart and J. Kennedy, "A new optimizer using particle swarm theory," in *Proc. 6th Int. Symp. Micro Mach. Hum. Sci.*, Nagoya, Japan, 1995, pp. 39–43.
[20] A. A. Heidari, S. Mirjalili, H. Faris, I. Aljarah, M. Mafarja, and H. Chen, "Harris hawks optimization: Algorithm and applications," *Future Gener. Comput. Syst.*, vol. 97, pp. 849–872, Aug. 2019.
[21] S. Mirjalili and A. Lewis, "The whale optimization algorithm," *Adv. Eng. Softw.*, vol. 95, pp. 51–67, May 2016.
[22] M. Farhadi-Kangarlu, E. Babaei, and F. Blaabjerg, "A comprehensive review of dynamic voltage restorers," *Int. J. Electr. Power Energy Syst.*, vol. 92, pp. 136–155, Nov. 2017.
[23] S. W. Middlekauff and E. R. Collins, "System and customer impact: Considerations for series custom power devices," *IEEE Trans. Power Del.*, vol. 13, no. 1, pp. 278–282, Jan. 1998.
[24] S. K. Chung, "Phase-locked loop for grid-connected three-phase power conversion systems," *IEE Proc.-Electr. Power Appl.*, vol. 147, no. 3, pp. 213–219, May 2000.
[25] S. Ekinci and B. Hekimoglu, "Improved kidney-inspired algorithm approach for tuning of PID controller in AVR system," *IEEE Access*, vol. 7, pp. 39935–39947, 2019.
[26] R. Çoban and Ö. Erçin, "Multi-objective bees algorithm to optimal tuning of PID controller," *Çukurova Univ. J. Fac. Eng. Archit.*, vol. 27, no. 2, pp. 13–26, 2012.
[27] D. E. Seborg, D. A. Mellichamp, and T. F. Edgar, *Process Dynamics and Control*. Hoboken, NJ, USA: Wiley, 2010.
[28] M. Settles, *An Introduction to Particle Swarm Optimization*. London, U.K.: Springer, 2005, pp. 1–8.
[29] M. A. Sobhy, M. Ezzat, H. M. Hasanien, and A. Y. Abdelaziz, "Harris hawks algorithm for automatic generation control of interconnected power systems," in *Proc. 21st Int. Middle East Power Syst. Conf. (MEPCON)*, Dec. 2019, pp. 575–582.
[30] X. Bao, H. Jia, and C. Lang, "A novel hybrid harris hawks optimization for color image multilevel thresholding segmentation," *IEEE Access*, vol. 7, pp. 76529–76546, 2019.
[31] R. Isermann, J. Schaffnit, and S. Sinsel, "Hardware-in-the-loop simulation for the design and testing of engine-control systems," *Control Eng. Pract.*, vol. 7, no. 5, pp. 643–653, May 1999.
[32] *Typhoon HIL402*. [Online]. Available: https://www.typhoon-hil.com/

ZEINAB ELKADY received the degree (Hons.) from the Electrical Engineering Department, Electric Power and Machines Program of the Faculty of Engineering, Benha University, Egypt, in May 2007, and the M.Sc. degree in electrical engineering (power system) from Benha University, in 2016. Her graduation project was "Standalone photovoltaic system design and implementation using FPGA" using sparten3-E which supplied to the project by XLINIX as a sponsor. She participated in ROBOCON competition and achieved two prizes in two years. She worked as a Researcher Assistant with the Electronic Research Institute (ERI). Her specific fields of interest include power system control, power quality, and renewable energy. She is currently an Assistant Researcher with the Electronics Research Institute-Egypt.

NASER ABDEL-RAHIM received the M.Eng. and Ph.D. degrees from the Memorial University of Newfoundland, Canada, in 1989 and 1995, respectively. He is currently a Professor with the Department of Electrical Engineering, Future University, Egypt. From 2013 to 2017, he had been a Professor with the Faculty of Engineering, Shoubra, Benha University, Egypt. As an Assistant Professor at the United Arab Emirates University (UAEU), from 2000 till 2005, he obtained several research projects funding from the UAEU as well as from Asea Brown Boveri (ABB). He has numerous publications in international journals and refereed conferences, where he also served as a reviewer.

AHMED A. MANSOUR was born in Qalubia, Egypt, in December 1967. He graduated from the Electrical Power and Machines Department of the Faculty of Engineering, Zagzig University, in May 1990. He received the M.Sc. and Ph.D. degrees from the Faculty of Engineering, Cairo University, in 1999 and 2004, respectively. His specific fields of interest include power electronics and power quality systems. His experience on advanced power factor correction techniques based on both Static Var Compensators ''SVC's'', STATCOM systems and Active Power Filters (APF's) systems dedicated to harmonics compensation of the electrical non-linear loads. He is currently working as an Associate Professor Researcher with the Power Electronics and Energy Conversion Systems Department, Electronics Research Institute, Egypt.

FAHMY. M. BENDARY received the B.Sc. degree from Ain Shams University, Egypt, and the M.Sc. degree from Cairo University, Egypt, in 1966 and 1979, respectively, and the Ph.D. degree from Paris, Sud University, France, in 1983. From 1984 to 1995, he was an Associate Professor with Zagazig University. He was promoted to full professor of automatic control and its applications to power system, in 1995. He is currently a Professor of electric power systems and automatic control at the faculty of engineering, Shoubra, Benha University. He is a coauthor of more than one hundred research articles, and a reviewer for many local and international journals as well as conferences in the field of power system optimization, operation, planning, control, and renewable energy systems.